Murdoch
UNIVERSITY

MURDOCH RESEARCH REPOSITORY

This is the author's final version of the work, as accepted for publication following peer review but without the publisher's layout or pagination. The definitive version is available at
http://dx.doi.org/10.1074/jbc.M113.497990

Hargrove, T.Y., Wawrzak, Z., Alexander, P.W., Chaplin, J.H., Keenan, M., Charman, S.A., Perez, C.J., Waterman, M.R., Chatelain, E. and Lepesheva, G.I. (2013) Complexes of Trypanosoma cruzi Sterol 14 -Demethylase (CYP51) with Two Pyridine-based Drug Candidates for Chagas Disease: Structural basis for pathogen selectivity. Journal of Biological Chemistry, 288 (44). pp. 31602-31615.

http://researchrepository.murdoch.edu.au/19447/

Copyright: © 2013 by The American Society for Biochemistry and Molecular Biology, Inc.

It is posted here for your personal use. No further distribution is permitted.

Complexes of *Trypanosoma cruzi* sterol 14a-demethylase (CYP51) with two pyridine-based drug candidates for Chagas disease: *Structural basis for pathogen-selectivity**

Tatiana Y. Hargrove[1], Zdzislaw Wawrzak[2], Paul W. Alexander[3], Jason H.Chaplin[3], Martine Keenan[3], Susan A. Charman[4], Catherine J. Perez[5], Michael R. Waterman[1], Eric Chatelain[6], Galina I. Lepesheva[1,7]

[1]From the Department of Biochemistry School of Medicine, Vanderbilt University, Nashville, TN, 37232, USA
[2]Synchrotron Research Center, Life Science Collaborative Access Team, Northwestern University, Argonne, IL, 60439, USA
[3]Epichem Pty Ltd, Murdoch University Campus, South Street, Murdoch, Western Australia 6150, Australia
[4]Centre for Drug Candidate Optimisation, Monash Institute of Pharmaceutical Sciences, Monash University, Parkville, Victoria 3052, Australia
[5]Department of Parasitology and Veterinary Sciences, Murdoch University, South Street, Murdoch, Western Australia 6150, Australia
[6]Drugs for Neglected Diseases initiative (DNDi), 15 Chemin Louis Dunant, 1202 Geneva, Switzerland
[7]Vanderbilt Center for Structural Biology and Institute for Global Health, Nashville, TN, 37232, USA

***Running title**: *T. cruzi* CYP51 complexes with UDO and UDD

To whom correspondence should be addressed: Galina I. Lepesheva, Department of Biochemistry School of Medicine, Vanderbilt University, 622 RRB, 23rd at Pierce, Nashville, TN, 37232, USA, Tel: 615-343-1373, Fax: 615-322-4349 Email: galina.i.lepesheva@vanderbilt.edu

Keywords: Cytochrome P450 (CYP), sterol 14α-demethylase (CYP51), inhibition, X-ray structure, *Trypanosoma cruzi*, Chagas disease

Background: Two pyridine derivatives were identified as promising drug candidates in animal models of Chagas disease.
Results: They were tested as sterol 14α-demethylase (CYP51) inhibitors; X-ray co-structures with *T. cruzi* CYP51 were determined.
Conclusion: The structures explain the compounds' potency and selectivity.
Significance: Structural information contributes to a better understanding of P450 inhibition and will facilitate rational design of pathogen-specific drugs.

ABSTRACT

Chagas disease, caused by the eukaryotic (protozoan) parasite *Trypanosoma cruzi*, is an alarming emerging global health problem with no clinical drugs available to treat the chronic stage. Azole inhibitors of sterol 14α-demethylase (CYP51) were proven effective against Chagas, and antifungal drugs posaconazole and ravuconazole entered clinical trials in Spain, Bolivia and Argentina. Here we present the X-ray structures of *T. cruzi* CYP51 in complexes with two alternative drug candidates, pyridine derivatives (S)-(4-chlorophenyl)-1-(4-(4-(trifluoromethyl)phenyl)-piperazin-1-yl)-2-(pyridin-3-yl)ethanone (PDB code UDO) and N-[4-(trifluoromethyl)phenyl]-N-[1-[5-(trifluoromethyl)-2-pyridyl]-4-piperidyl]pyridin-3-amine (UDD). These compounds have been developed by Drugs for Neglected Diseases initiative (DNDi) **and are highly promising antichagasic agents, both in cellular and *in vivo* experiments. Binding parameters and inhibitory effects on sterol 14α-demethylase activity in reconstituted enzyme reactions confirm UDO and UDD as potent and selective *T. cruzi* CYP51 inhibitors. Comparative analysis of the pyridine- and azole-bound CYP51 structures uncovers the features which make UDO and UDD *T. cruzi* CYP51 specific. The structures suggest that while precise fit between the shape of the inhibitor molecules and *T. cruzi* CYP51 active**

Copyright 2013 by The American Society for Biochemistry and Molecular Biology, Inc.

site topology underlies their high inhibitory potency, a longer coordination bond between the catalytic heme iron and the pyridine nitrogen implies weaker influence of pyridines on the iron reduction potential, which may be the basis for the observed selectivity of these compounds towards the target enzyme versus other CYPs, including human drug-metabolizing P450s. The findings might pave the way for the development of novel CYP51-targeted drugs with optimized metabolic properties that are highly needed for treatment of human infections caused by eukaryotic microbial pathogens.

Sterol 14α-demethylase (CYP51) is a cysteine-coordinated hemoprotein, the cytochrome P450 (CYP) monooxygenase that catalyses the three-step reaction of oxidative removal of the 14α-methyl group from cyclized sterol precursors (1,2). This P450 enzyme is found in all kingdoms of life (3,4), its reaction being essential for sterol biosynthesis (5). The products of the pathway, such as cholesterol in humans or ergosterol in fungi, are required for the integrity of the eukaryotic cell membrane and as metabolic precursors for a variety of signaling molecules. For more than 40 years CYP51 has successfully served as the major target for antifungal azoles (6-8), and by now it is quite generally recognized as a promising therapeutic target in *Trypanosoma (T.) cruzi* as well (9).

Endemic in South America, Chagas disease is a life threatening malignancy with only two drugs available for treatment (benznidazole and nifurtimox), both having low efficiency for the chronic stage that predominantly affects the heart and gastrointestinal tract. The disease is now becoming a severe global health problem, mainly due to human migration to other continents but also because of the broadening of the area of vector habitat: the triatomine insects that transmit the parasite (kissing bugs) now populate two-thirds of the US land (10) and have been found in Asia, Australia and Africa. However, historically known as a disease of the poor, the infection does not attract the attention of pharmaceutical companies as being profitable, and for more than a century since its discovery the parasite has remained incurable.

Finally, in 2011, after ~30 years of effort from academia on antifungal drug repurposing (11-17), two antifungal azoles, posaconazole and ravuconazole, entered clinical trials for Chagas disease (18). Some other azoles, such as the derivatives of the anticancer drug candidate tipifarnib (19,20) or FTI-2220 (21) were shown to display potent antiparasitic effects and are under investigation. Furthermore, an experimental *T. cruzi* CYP51 inhibitor VNI has been recently proven to cure both the acute and chronic forms of Chagas disease in mice (22).

Similar to fungi, in *T. cruzi* the endogenously synthesized sterol molecules are C24-alkylated (ergosterol-like) and therefore they cannot be replaced in the parasite cells by host cholesterol (23). The shortage of endogenous sterols is especially harmful for the multiplying form of *T. cruzi,* intracellular amastigotes (24), the morphological form of the parasite that is prevalent at the chronic stage of infection. Accordingly, in amastigotes the expression level of the CYP51 gene is higher (25), and the effect of CYP51 inhibitors is about 3 orders of magnitude stronger than in the non-multiplying bloodstream trypomastigotes (22,25,26), the forms that are more relevant to the acute stage of infection and can be effectively treated with benznidazole. Depletion of endogenous sterols in *T. cruzi* due to CYP51 inhibition causes blebbing of the cellular membrane, mitochondrial swelling, alterations in endoplasmic reticulum and Golgi, nuclear envelope detachment, deterioration of internal membranes and ultimately results in cell lysis and death (27,28).

T. cruzi CYP51, which has <25% identity to fungal orthologs, has been well characterized biochemically and structurally (25-27,29). First, the gene was cloned from the Tulahuen strain of the pathogen, the recombinant protein expressed in *Escherichia coli* and purified (29). We found that the *T. cruzi* CYP51 substrate preference towards the C4-double methylated eburicol (24-methylene-dihydrolanosterol) is largely defined by a single amino acid residue in the B' helix, I105 (animal/fungi-like), versus the corresponding Phe in the plant-like CYP51 orthologs from *T. brucei* (30) and *Leishmania (L.) infantum* (31) that catalyze 14α-demethylation of C4-monomethylated obtusifoliol and norlanosterol. Studies on CYP51 inhibition revealed that susceptibilities of the protozoan enzymes to antifungal drugs often differ significantly from

those of fungal CYP51 orthologs and led to identification of several novel experimental inhibitory scaffolds (26,27,32,33). Determination of X-ray crystal structures of *T. cruzi* (25,34), *T. brucei* (20,35) and *L. infantum* (31) CYP51s, ligand-free and complexed with several azole derivatives including 1,2,4-triazole posaconazole (25) and 1,3-imidazole VNI (35), and with the mechanism-based suicide substrate 14α-methylenecyclopropyl-dihydrolanosterol (32) established the molecular basis for the CYP51 catalytic conservation (36). To be able to perform its ancient biological function across phylogeny at very low sequence identity, this P450 enzyme has a highly rigid substrate binding cavity, which in turn serves as the foundation for its druggability (32,37).

In the present work we tested *T. cruzi* CYP51 as a potential target for two pyridine-based compounds, EPL-BS1246 (UDO) and EPL-BS0967 (UDD), which have been identified as strong antiparasitic agents in cellular *T. cruzi* experiments and display high potency *in vivo* in a stringent mouse model of Chagas disease. We report UDO and UDD binding parameters, inhibitory effects on sterol 14α-demethylation activity and co-structures with *T. cruzi* CYP51, comparing them with the CYP51 complexes with posaconazole and VNI (Fig. 1). The structures provide valuable information regarding the features that contribute to the potency of these two new CYP51 inhibitors and their selectivity towards the *T. cruzi* enzyme ortholog. Particularly, they show that the peculiarities observed in the enzyme spectral responses to UDO/UDD binding reflect a longer coordination bond between the ferric heme iron and heterocyclic pyridine (vs. azole) nitrogen, which is likely to underlie higher specificity because weakened Fe-N interaction would enhance the role of other, non-bonded protein-ligand contacts. This is the first report of highly potent *T. cruzi* CYP51 inhibitors of non-azole nature, and we believe that the information gained in this study will facilitate structure-based design of pathogen-specific drugs with optimized metabolic properties, which will have little or no effect on human drug-metabolizing P450s.

EXPERIMENTAL PROCEDURES

Testing UDO (EPL-BS1246) and UDD (EPL-BS0967) as antiprotozoan drug candidates.

The compounds – UDO and UDD were synthesized as part of a Drugs for Neglected Diseases initiative (DNDi) drug discovery program to develop new treatments for Chagas disease and are the result of structure-activity relationship (SAR) optimization of plant fungicide fenarimol (pyrimidine derivative), which was found to have moderate *in vitro* activity against *T. cruzi* (38). The synthesis was carried out by analogy to the methods reported in (38,39). Both compounds were prepared by a short synthetic sequence from readily available precursors. Racemic-UDO was synthesized in 5 steps (3 contiguous) from key building blocks 3-fluoropyridine, 4-chlorophenylacetonitrile and 1-[4-(trifluoromethyl)phenyl]piperazine in high overall yield (45%). Chiral resolution was achieved using supercritical fluid chromatography (SFC) after which the *S*-enantiomer was identified as most active in *in vitro* assays. UDD was constructed in 4 steps, 12% overall yield, from 3-amino pyridine, piperidin-4-one and 2-chloro-5-(trifluoromethyl)pyridine. As a trigonal N-centered ligand, UDD is achiral and no further manipulation of the final product was required.

Cellular T. cruzi assay - The assay was performed using the β-galactosidase expressing Tulahuen *T. cruzi* as described previously (40). Briefly, L6 cells were plated into 96 well, flat-bottom tissue culture plates and incubated at 37°C in 5% CO_2 for 24 h to allow cells to adhere. *T. cruzi* trypomastigotes were then added at a multiplicity of infection of 3, and plates were incubated for a further 48 h to allow infection to establish. Extracellular trypomastigotes were then removed and compounds were added in seven-point serial dilutions performed in triplicate. After 96 h of incubation with the compounds, chlorophenol red-fl-D-galactopyranoside (CPRG, Roche) was added; a color change following catabolization of the reagent by viable *T. cruzi* was observed and absorbance was read at 530 nm using a Dynex microplate reader.

Cellular L. donovani assay – The assay was performed using the *L. donovani* MHOM/ET/67/ L82 strain. Primary peritoneal mouse macrophages were infected at a multiplicity of infection of 1 to 10 with *Leishmania* parasites. Compounds were added after 2 hours of infection. Parasite multiplication was compared to untreated-infected controls (100% growth) and uninfected controls

(0% growth). After 5 days incubation, parasite burdens (mean number of amastigotes per macrophage) were microscopically assessed after staining the cells with a 10% Giemsa solution. The results were expressed as % reduction in parasite burden compared to untreated control wells.

Anti-T. cruzi activity in vivo - Female Swiss mice ~8 weeks old were obtained from the Animal Resources Centre (Perth, Western Australia). All animal experiments were carried out with approval of the Animal Ethics Committee of Murdoch University as described (38). Briefly, compounds were suspended in a hydroxypropylmethyl-cellulose suspension vehicle (0.5% w/v hydroxyl-propylmethylcellulose + 0.4% v/v Tween 80 + 0.5% v/v benzyl alcohol in deionized water) and given by oral gavage. Induction of acute *T. cruzi* infection was achieved by infecting mice with 50,000 Tulahuen trypomastigotes via intraperito-neal (ip) injection (5 mice per group). Compound administration was commenced on day 8 post infection and continued daily for 20 days. Parasitemia was determined by collection of blood by tail prick and counting live trypomastigotes under the microscope using a Neubauer hemocytometer. Efficacy was monitored by comparison of parasitemia levels in compound treated vs. vehicle only treated groups. If parasitemia levels were no longer detectable in the blood following compound treatment, animals were immunosuppresed with cyclophosphamide 10 days after the treatment cessation. Cyclophosphamide was administered ip at 50 mg/kg/day in three cycles; each cycle comprised 4 days treatment followed by 3 days rest. Parasitemia was determined by collection of blood as detailed above; parasitological cure was confirmed by PCR on tissue samples (38). More extended description of *in vivo* data will be published elsewhere.

Inhibition of human drug-metabolizing CYPs - Inhibition of hepatic cytochromes P450 was assessed in human liver microsomes using a substrate specific approach monitoring metabolites formed by each specific CYP enzyme. Metabolic reactions included phenacetin-O-deethylation (1A2), tolbutamide methylhydroxylation (2C9), S-mephenytoin 4'-hydroxylation (2C19), dextrome-thorphan O-deethylation (2D6), and testosterone-6-β-hydroxylation (3A4). Each substrate was added at a concentration less than or equal to the Km for the metabolic pathway, and microsomal protein concentrations and assay incubation times were optimized for each reaction to ensure linear metabolite formation based on initial rates (Table 1). Microsomes were suspended in phosphate buffer and incubated at 37ºC in the presence of probe substrates. Reactions were initiated by the addition of an NADPH-regenerating buffer system and were quenched at appropriate times using acetonitrile. Samples were centrifuged and concentrations of metabolites assessed by LC/MS. The IC_{50} was taken as the concentration at which there was a 50% reduction in the rate of metabolite formation relative to the metabolite formation rate in the absence of inhibitor. Additionally, effects of UDO and UDD on CYP3A4 were compared with the effects of posaconazole and VNI (Fig. 1) using a commercial kit (BD Biosciences Screening Kit) as described (22), drug concentration range 16000-2.4 nM. IC_{50} for the manufacturer's positive control inhibitor ketoconazole at these conditions was ~ 8 nM).

Testing UDO (EPL-BS1246) and UDD (EPL-BS0967) as CYP51 inhibitors.

Protein engineering, expression and purification - For functional studies, including ligand binding and enzymatic activity assays, the full-length CYP51 expression constructs, designed as described in (29,31), GenBank IDs AY856083 and EF192938 for *T. cruzi* and *L. infantum* CYP51, respectively, were used. For crystallization, we utilized the *T. cruzi* CYP51 N-terminal truncated construct where the membrane anchor sequence (first 31 residues upstream of P32) was replaced with the 5-amino acid sequence fragment MAKKT- described in (25) for co-crystallization with posaconazole. In all cases the CYP51 genes were His-tag-engineered at the C-terminus to facilitate purification, subcloned into the pCW expression vector at Nde I (5'-) and Hind III (3') sites and expressed in *E. coli* strain HMS174(DE3) (Novagen). For *T. cruzi* CYP51, purification procedure included sequential chromatography on nickel nitrotriloacetate-agarose (Qiagen) and carboxymethyl-Sepharose (Sigma) (29). *L. infantum* CYP51, human CYP51 and cytochrome P450 reductase were purified as previously reported (30,31,41). For crystallization purposes complexes with the inhibitors were obtained by saturating *T. cruzi* CYP51 with the

compound during the last purification step by adding a 10 mM DMSO stock solution of the inhibitor to the washing and elution buffers, final concentration being 20 μM.

Spectral ligand binding assay – All spectra were recorded at 22ºC on a dual-beam Shimadzu UV-240IPC spectrophotometer. The P450 concentration was determined from the Soret band intensity of the reduced CO complexes using visible absorption difference spectroscopy, $\Delta\varepsilon_{450-490} = 91\ mM^{-1}cm^{-1}$ (42). Spectral titrations were carried out at 0.4 μM P450 concentration in a 50 mM K-phosphate buffer, pH 7.4, containing 200 mM NaCl and 0.1 mM EDTA. The optical path length was 5 cm. Ligand binding was monitored as a red shift in the Soret band maximum reflecting coordination of the heterocyclic nitrogen to the P450 heme iron (26). Difference spectra were generated by recording the P450 absorbance in a sample cuvette versus the absorbance in a reference cuvette, both containing the same amount of the protein. Compounds were added to the sample cuvette in the concentration range 0.1 - 2.0 μM from 0.2 mM stock solutions in DMSO. The titration step was 0.1 μM. At each step, the corresponding volume of DMSO was added to the reference cuvette. The apparent dissociation constants of the enzyme-inhibitor complexes (K_d) and the maximum spectral change (ΔA_{max}) were calculated using a quadratic function for tight binding ligands by fitting the data for the ligand-induced spectral change (peak to trough absorbance changes in the difference spectra (ΔA)) versus total ligand concentration to the following equation (43) in Prism (GraphPad Software):

$$\Delta A=(\Delta A_{max}/2E)((L+E+K_d)-((L+E+K_d)^2-4LE)^{0.5}),$$

where [L] and [E] are the concentrations of the ligand and the enzyme used for the titration, respectively.

CYP51 inhibition assay - Enzymatic activity of *T. cruzi*, *L. infantum* and human CYP51s was reconstituted *in vitro* as described previously (29,31,41), using eburicol, obtusifoliol and lanosterol, respectively, as the substrates. Briefly, the reaction mixture contained 1 μM CYP51, 2 μM cytochrome P450 reductase (CPR), 100 μM dilauroyl-α-phosphatidylcholine, 0.4 mg/ml isoctrate dehydrogenase and 25 mM sodium isocitrate in 20 mM MOPS (pH 7.4), 50 m M KCl, 5 mM $MgCl_2$ and 10% glycerol. After addition of the [^{3}H]-radiolabeled sterol substrate (~2,000 cpm/nmol, final concentration 50 μM) the mixture was preincubated for 5 min at 37 ºC in a shaking water bath (GCA Precision Scientific). The reaction was initiated by addition of 100 μM NADPH and stopped by extraction of the sterols with ethyl acetate. The reaction products were dried, dissolved in methanol and analyzed by a reverse-phase HPLC system (Waters) equipped with β-RAM detector (INUS Systems, Inc.) using a Nova Pak C18 column (particle size 4 μM, 3.9 x 150 mm) and linear gradient water:acetonitrile:methanol (1.0:4.5:4.5) (solvent A) methanol (solvent B) at a flow rate 1 ml/min. At these conditions the retention time for eburicol, obtusifoliol and lanosterol was 26, 23, and 25 min, respectively. Retention time for the reaction intermediates, 14α-alcohol and 14α-aldehyde derivatives of obtusifoliol (30) (seen in Fig. 3, *L. infantum* CYP51), was 10 and 12 min, respectively. Potencies of UDO and UDD to inhibit *T. cruzi*, *L. infantum* and human CYP51 were compared as inhibition of enzymatic activity in a one hour reaction (25,26), posaconazole serving as positive control.

Crystallization, Data Collection and Structure Determination - The co-crystals were obtained by hanging drop vapor diffusion. The 250 μM protein solution in 20 mM K-phosphate buffer, pH 7.2, containing 200 mM NaCl, 0.1 mM EDTA, 1 mM dithiothreitol, 10% glycerol and 8 mM Cymal 4, saturated with the inhibitor as described above, was mixed with the equal volume of a precipitant solution containing 50 mM K-phosphate buffer, pH 7.6, 0.2 M magnesium chloride hexahydrate and 25% (w/v) PEG 4000 and was equilibrated against the precipitant solution at 22ºC. Crystals were prescreened using Bruker Microstar microfocus rotating-anode X-ray generator/Proteum PT135 CCD area detectors, and those that diffracted to ~3.0Å resolution were subsequently used for the data collection at a synchrotron (Advanced Photon Source, Argonne National Laboratory, IL). Data were collected at LS-CAT, beamline 21ID-F. The diffraction images were integrated using Mosflm (44) and scaled with Aimless (CCP4 Program Suite 6.3.0 (45)) in the P3(1)21 space group to resolutions of 2.8 Å (UDO) and 2.9 Å (UDD). Solvent content was

estimated with Matthews probability calculator. In both cases a single solution with one molecule in the asymmetric unit was found with PhaserMR using posaconazole-bound *T. cruzi* CYP51 structure (PDB code 3K1O) as the search model. Iterative models of the protein-inhibitor complexes were built and refined using COOT (46) and Refmac (47) in CCP4 (45). The statistics for data collection, refinement, and validation are shown in Table 2. The protein chain is seen from residue 28 (A in the N-terminal MAKKT- sequence) to 478 (of 482) for *T. cruzi* CYP51-UDO and from residue 29 to 478 for *T. cruzi* CYP51-UDD. The electron density for both UDO and UDD was well defined (Fig. 2), showing single orientation of the inhibitor molecule within the enzyme binding cavity and full occupancy. The coordinates and structure factors have been deposited at the Protein Data Bank, PDB codes 3zg2 (CYP51-UDO) and 3zg3 (CYP51-UDD).

RESULTS

As shown in Fig. 1, UDO and UDD are highly efficient against *T. cruzi*, both in cellular experiments and *in vivo*. The compounds were identified upon testing of a number of pharmacologically optimized derivatives of pyrimidine-based fungicide fenarimol and both contain a heterocyclic (pyridine) ring with a basic nitrogen atom, thus suggesting a possibility of its coordination to the P450 heme iron. On the other hand, their inhibitory effects on all five major human drug-metabolizing P450s (48) are very weak (Table 1), and the whole organism primary *in vitro* screen that was used to drive the discovery process is mechanistically nonspecific. Therefore, it was of special interest to verify whether they inhibit the parasite CYP51.

CYP51 spectral responses to ligand binding. Recombinant CYP51s are usually purified in the hexacoordinated low spin form, with the Soret (γ) band absorbance maximum at ~417 nm (3,29-31,49), the oxygen atom from a water molecule serving as the sixth (distal axial) ligand for the ferric heme iron (50). If a stronger ligand replaces the water molecule in the iron coordination sphere, the Soret maximum shifts to the longer wavelength (red shift, or type II spectral response). Consequently, in the difference spectra a trough and a peak appear on the left and the right side of an isosbestic point, respectively. Accordingly, when the iron in *T. cruzi* CYP51 becomes coordinated to an azole ring nitrogen, the trough/isosbestic point/peak in the difference spectra emerge at 407/419/428 nm in the case of imidazole N3 (VNI) (Fig. 3D) and at 392/415/425 nm in the case of triazole N4 (posaconazole) (Fig. 3C). The difference spectra elicited in *T. cruzi* CYP51 by UDO and UDD, however, revealed the trough at 389 nm, isosbestic point at 411 nm and peak at 423 and 422 nm, respectively (Fig. 3A,B). The Soret band absolute absorbance maximum was red-shifted only to 421 nm (vs. 424 nm in VNI-bound and 423 nm in posaconazole-bound CYP51 (Table 3)), hence suggesting weaker interaction of the sixth ligand with the heme iron. On the other hand, the apparent K_d values calculated from *T. cruzi* CYP51 spectral responses to UDO (19 nM) and UDD (32 nM) were found comparable to those obtained for VNI and posaconazole (Table 3), the titration curves all showing saturation at about equimolar ratio inhibitor/enzyme (Fig. 3A). Thus, although the pyridine ring nitrogen can be characterized as a weaker iron-coordinating atom, based on the apparent K_d values, both compounds seemed to form strong complexes with *T. cruzi* CYP51. Interestingly, for *L. infantum* CYP51, whose spectral responses to the binding of UDO and UDD are quite similar in their shape (Fig. 3E,F), the calculated K_ds were about one order of magnitude higher, 156 nM and 419 nM, respectively (Table 3), while the responses of the human enzyme ortholog suggested tight binding with the position of the peak in the difference spectra red-shifted to 424 nm (Fig. 3G,H) and the apparent K_ds of 69 nM (UDO) and 26 nM (UDD) (Table 3).

Inhibition of CYP51 activity *in vitro*. As discussed previously (26,37), sensitivity of the CYP51 reaction reconstituted *in vitro* is limited by a) the affinity of the CYP51-CPR complex formation (Kd ≈1 μM, so that further lowering the P450 concentration sharply decreases its turnover rate) and b) by very poor solubility of the sterol substrates which in turn does not allow the use of higher substrate excess over the enzyme. Therefore, in order to identify most potent CYP51 inhibitors, in our standard conditions we use a one hour CYP51 reaction, the molar ratio inhibitor/enzyme/substrate being 2/1/50 (20,25,34). At these conditions, in the absence of

inhibitors all the substrate is converted into the product, and most compounds (even amongst those displaying complete inhibition of the initial rate of the reaction) show little inhibitory effect (9) because over time they are replaced in the enzyme active center by substrate.

-*T. cruzi CYP51*. UDO and UDD, however, completely inhibit *T. cruzi* CYP51 activity under these conditions (Fig. 4A,B). Moreover, lowering the concentration of *T. cruzi* CYP51 in the reaction mixture to 0.2 μM (which leads to about a 40-fold decrease in the enzyme turnover) did not reveal any product formation at inhibitor/enzyme molar ratios ≥1 in all three cases (not shown). These data indicate that although based on the position of the Soret band maximum Fe-pyridine interaction can be characterized as weaker, potencies of these compounds to inhibit the *T. cruzi* enzyme activity are similar to that of posaconazole and agree with the low apparent K_d values.

-*L. infantum CYP51*. The inhibitory effects of both compounds on the activity of *L. infantum* CYP51 are slightly weaker, as 32% and 60% of substrate conversion is observed at a two-fold molar excess of UDO and UDD, respectively (Fig. 4A); the molar ratios inhibitor/enzyme required to slow down the *L. infantum* CYP51 reaction 2-fold are 1.5 and 2.8 (Fig. 4C). Again, lower inhibitory potencies correlate with the lower apparent binding affinities and are in agreement with the weaker antiparasitic effect of UDD against leishmania cells (Fig. 1).

-*Human CYP51*. The activity of the human enzyme, however, is not affected at these conditions: a 180-fold molar excess of UDO and a 35-fold molar excess of UDD were necessary to achieve a 2-fold inhibition (Fig. 4D). Thus, regardless of the low apparent K_ds calculated from the titration curves, both compounds (especially UDO) inhibit human CYP51 much weaker than the parasitic counterparts.

Interestingly, relative potencies of UDO and UDD to inhibit human and leishmania CYP51s are reversed: while UDO is roughly 2-fold stronger than UDD as the inhibitor of *L. infantum* CYP51, for the human enzyme UDD has a 5-fold higher potency than UDO. In order to better understand the molecular basis for the compounds potency/selectivity, we determined their X-ray structures in complexes with *T. cruzi* CYP51.

Structural characterization of the CYP51-inhibitor complexes.

-*Inhibitor binding mode.* As expected for type II P450 ligands, each of the inhibitors interacts with the heme, its pyridine ring nitrogen forming a coordination bond to the heme iron. The pyridine rings are in favorable conformation, perpendicular to the heme plane. Yet, in both cases the Fe^{3+}-N coordination bond is rather long, 2.31Å for UDO and 2.34Å for UDD (Fig. 2). This is about 0.3 Å longer than the coordination bond in the CYP51 complexes with imidazoles (2.0-2.04Å in VNI [3gw9](35), tipifarnib derivative JFK [3tik] (20) or NEE [4h6o] (34),) and more than 0.2Å longer than the coordination bond in the CYP51 complexes with triazoles (2.07-2.15 Å) [3k1o], [3khm] (25) or [3l4d] (31) (see examples in Table 4). A weaker coordination bond explains the smaller red shift in the Soret band absorbance maximum and apparently reflects the decrease in the elecronegativity of the iron-coordinating atom (imidazole > triazole > pyridine). Overall, orientation of UDO and UDD within the CYP51 binding cavity is similar to VNI and almost identical to that of posaconazole, with the longer (two-ring) arm of each compound being directed towards the substrate access channel entrance (Fig.5. A,B,C).

-*Overall CYP51 structure.* Similar to what was observed previously for complexes with imidazole and triazole inhibitors (20,25,34,35) and the substrate analog MCP (32), binding of UDO or UDD does not induce any significant conformational changes at the overall structure level (Fig. 5D). The root mean square deviations (rmsd) for Cα atoms of 3zg2 and 3zg3 relative to 3k1o (posaconazole bound *T. cruzi* CYP51) are only 0.535Å and 0.567Å, respectively, and between the two structures reported here the rmsd is 0.453 Å. As appears to be common for CYP51s, the highest deviations are displayed by a few residues at the N- and C-termini, the GH loop region as well as by the structural elements surrounding the entrance into the substrate access channel, especially the FG loop area. While the functional role of the GH loop flexibility in CYP51s remains unclear, the movements around the F'' helix, which forms the upper portion (the lid) of the substrate channel entrance, may reflect opening and closing of the channel that takes place *in vivo,* upon binding of the bulky sterol molecule

and release of the 14α-demethylated reaction product back into the microsomal membrane. The other secondary structural elements, including the side chains of the residues contacting the inhibitor, remain in very similar positions in both structures (the stereoview of their superimposition can be seen in Fig. 6C).

-*UDO-CYP51 complex.* UDO (MW 460, 16.5 Å in length) has the molecular volume of 549 $Å^3$ (Accelrys), which is considerably smaller than the volume of Pos (673 $Å^3$, 25.5 Å in length (25). Nevertheless, it forms van der Waals contacts with 18 amino acid residues (the distance <4.5 Å) of the enzyme (Fig. 6A). Six of these residues, V102, Y103, M106, F110, A115 and Y116, are from the B' helix and B'/C loop, the major CYP51 substrate recognition site. In the sterol-bound form of the enzyme, these secondary structural elements encircle the whole skeleton of the substrate molecule from its β-side (32). L127 is from helix C (CYP51-specific area of the binding cavity). In the substrate-bound CYP51 it interacts with the distal portion of the sterol arm (C26-C28). Altogether, these seven residues flank the inhibitor from the upper portion of the enzyme active site. Helix I forms the distal wall of the cavity and provides 4 residues, A287, F290, A291, and T295. L356, M358 and M360 are from the K/β1-4 loop, and M460 is from the tip of the β4 hairpin, which also forms the bottom of the entrance into the substrate access channel. Again, the majority of these residues are involved into the interaction with the substrate (32) and reveal a high level of conservation within phyla, (36) thus providing a potential molecular basis for phyla-specificity of CYP51 inhibitors. Finally, P210, V213 and F214 (F'' helix) are from the lid of the substrate channel entrance. The involvement of these three residues is specific for UDO binding (left upper corner of Fig. 6A).

-*UDD-CYP51 complex.* UDD (MW 466, 15.6 Å in length) is even slightly smaller than UDO (molecular volume 535 $Å^3$), but it also forms van der Waals contacts with 18 amino acid residues, and again, only three of those residues, I105 (B' helix), L130 (C helix) and M284 (I helix), are UDD-specific (Fig. 6B). L130 and M284 are seen in the right lower corner of Fig. 6B, and 105 is the residue that defines the *T. cruzi* CYP51 substrate preference towards the C4-double methylated sterol substrates (29). In the *T. cruzi* CYP51 complex with UDD I105 is involved into the interaction with the inhibitor because, as it can be seen in Fig. 5A, the UDD molecule, whose structural skeleton is even more rigid than that of UDO, is slightly more crescent shaped. Another feature, specific to UDD *T. cruzi* CYP51 co-structure, is that the trifluoromethylbenzene ring of the inhibitor wedges between the heme plane and B'C loop, pushing away Y116 (Fig. 6D, right). Due to its offset position (4.02 Å) from the hydroxyl group of the porphyrin ring D propionate, the OH of Y116 cannot donate a hydrogen bond to the heme as it does in the enzyme complex with UDO (Fig. 6D, left) as well as with posaconazole (25). Displacement of the Y116 side chain was observed in the co-structures of *T. cruzi* CYP51 with VNF (25) and NEE (34). As discussed previously (35,36), disruption of this heme support from the protein moiety may also add to the UDD inhibitory potency. Assuming that the inhibitor molecule in human CYP51 adopts the orientation similar to that in the complex with *T. cruzi* CYP51, relatively stronger inhibition of the enzyme by UDD might also be due to disruption of the heme support from the corresponding Y (Y145 in human CYP51).

To summarize, binding of both UDO and UDD to *T. cruzi* CYP51 produces the enzyme-inhibitor complexes that display long Fe-N coordination bonds, extensive van der Waals interactions with the amino acid side chains of the active site and do not require structural rearrangements in the protein.

DISCUSSION

It has been known for years that cytochromes P450 are inhibited by heterocyclic compounds, with two components being important for the strength of the inhibition: 1) coordination of a basic heterocyclic atom with the heme iron (which lowers the P450 potential to be reduced) and 2) weaker but multiple interactions of the non-coordinated portion of the inhibitor molecule with the protein moiety (51). To date, within this type of P450 inhibitors, azoles have certainly remained the most potent, 1,3-imidazole and 1,2,4-triazole derivatives serving as clinical antifungal drugs and agricultural fungicides (CYP51 inhibition), and yet, especially within the last decade, becoming quite notorious for their off-target activity (particularly, inhibition of other human CYPs

(48,52-57), and relatively high propensity to induce resistance (58,59). Although several heterocyclic compounds other than azoles have been identified as *T. cruzi* CYP51 inhibitors, their inhibitory effects on the enzyme activity *in vitro* are much weaker, e.g. ChemDiv C155-0123 or indomethacin–pyridines are quite easily replaced by substrate during the time-course of the CYP51 reaction (9). To our knowledge, this is the first report of non-azole type II ligands whose potency to inhibit CYP51 activity is comparable with that of the most effective azoles (Fig. 4A).

This structural study suggests that because of weaker interaction between the heme iron and pyridine nitrogen of the inhibitors, the strength and selectivity of UDO and UDD must mainly derive from the fine topological fit between the rigid small molecules and *T. cruzi* CYP51 binding cavity. Thus, being much smaller than posaconazole, both UDO and UDD form contacts with as many as 18 amino acids within the *T. cruzi* CYP51 active site. Amongst them, the residues from the C-terminal portion of the B'/C loop, helix C and the N-terminal helix I (Fig. 6A,B) might be of special value to ensure CYP51-selectivity because this part of the cavity appears to be CYP51-specific (31,32). For comparison, posaconazole forms contacts with 24 amino acids of *T. cruzi* CYP51. Yet only 13 of these are from the CYP51 active site cavity, while the 11 others are located on the protein surface, encircling the entrance into the substrate access channel (25). Mutations in some of these residues were shown to be responsible for the development of CYP51-based posaconazole resistance in fungi (25). Besides, it is the synthesis of the posaconazole long arm (which in the enzyme/inhibitor complex protrudes through the channel entrance above the protein surface) that makes the drug highly expensive (60). VNI (35), whose molecular volume is comparable with UDO/UDD, forms contacts with only 15 protein residues; its potency/selectivity towards trypanosomal CYP51s, being strengthened by the hydrogen bond network that connects, via the inhibitor carboxamide fragment, the B' and I helices in the protozoan enzymes, but is probably not formed in the complex of VNI with the human CYP51 (9).

The notion that good fit between the non-ligated portions of UDO/UDD and the topology of the CYP51 binding cavity should play a greater role in these complexes is also supported by the results on inhibition of *L. infantum* and human CYP51s. In the *L. infantum* ortholog, which has a single amino acid difference from *T. cruzi* CYP51 within the active site, F104 (corresponding to I105 in *T. cruzi* (31)) protrudes deeper into the substrate binding cavity. In the *L. infantum* ortholog (one amino acid difference from *T. cruzi* CYP51 within the active site), the phyla-specific F104 (corresponding to *T. cruzi* CYP51 I105) protrudes deeper into the substrate binding cavity. When *L. infantum* and *T. cruzi* CYP51 structures are superimposed, it is seen that this residue comes into a close contact with UDO and especially with UDD (see Fig. 7A as an example). The distance F103-UDO (2.1Å) is too short, and would induce a strongly repulsive van der Waals potential between the contacting atoms. Hence, in the complex with *L. infantum* CYP51, the inhibitor molecule must adopt a slightly different position. As a result, the geometric fit is impaired, and the inhibitory potency decreases (Fig. 4A,C), which is also reflected in the lower binding affinity. On the contrary, the inhibitory effects of UDD and especially UDO on human CYP51 (where 12 of the 25 amino acids whose side chains line the surface of the active site cavity differ from those in *T. cruzi* CYP51 (Fig. 7B)) are negligible (Fig. 4D), although their binding affinities appear to be very high. This apparent discrepancy (low apparent K_ds yet weak inhibition) was observed before for other inhibitory scaffolds (e.g. posaconazole, VNF (25), VNI (35)) and can result from the differences in the central portion of the human CYP51 I helix (25,37) that has a low energy loop-like region preceded by a leucine residue (L310) instead of bulkier F290 in the parasitic CYP51s (Fig. 7B). Larger space combined with the elevated flexibility of the P450 core helix in close proximity to the heme iron area might diminish steric hindrances for a heterocyclic ring of an inhibitor to approach the heme, but will not be helpful in holding it within the P450 active center tight enough to prevent its replacement with the substrate in the enzymatic reaction.

Finally, a weaker coordination bond between the catalytic heme iron and the less electronegative nitrogen of the pyridine ring implies less negative impact of UDO and UDD on the P450 reduction potential. This provides a reasonable explanation for the observed weak influence of UDO and UDD

on the activity of the five major human drug-metabolizing P450s (Fig. 1, Table 1), a feature highly desirable for any new chemotherapeutic agents as it decreases the risk of potential *in vivo* toxicity, particularly due to adverse drug-drug interactions (48).

To conclude, UDO and UDD are promising new drug candidates for Chagas disease chemotherapy. Although their testing against other *T. cruzi* strains (which were recently shown to display high variability in their CYP51 genes (28)) is required prior to proceed to clinical trials, the compounds represent a valuable alternative as a new CYP51 inhibitory chemotype. The structural information gained in this study will provide guidance on the options for the scaffolds further improvement and analysis of their structure-activity relations. More general, the data suggest that balancing the impact of heme-heterocycle and apoprotein-ligand interactions may be highly helpful to minimize off-target activity of CYP51 inhibitors and subsequently to direct design of pathogen-selective drugs.

References

1. Fischer, R. T., Stam, S. H., Johnson, P. R., Ko, S. S., Magolda, R. L., Gaylor, J. L., and Trzaskos, J. M. (1989) Mechanistic studies of lanosterol 14 alpha-methyl demethylase: substrate requirements for the component reactions catalyzed by a single cytochrome P-450 isozyme. *J Lipid Res* **30**, 1621-1632
2. Trzaskos, J. M., Bowen, W. D., Shafiee, A., Fischer, R. T., and Gaylor, J. L. (1984) Cytochrome P-450-dependent oxidation of lanosterol in cholesterol biosynthesis. Microsomal electron transport and C-32 demethylation. *J Biol Chem* **259**, 13402-13412
3. Lepesheva, G. I., and Waterman, M. R. (2004) CYP51--the omnipotent P450. *Mol Cell Endocrinol* **215**, 165-170
4. Lepesheva, G. I., and Waterman, M. R. (2007) Sterol 14alpha-demethylase cytochrome P450 (CYP51), a P450 in all biological kingdoms. *Biochim Biophys Acta* **1770**, 467-477
5. Nes, W. R., and McKean, M. R. (eds). (1977) *Biochemistry of Steroids and other Isopentenoids*, University Park Press, Baltimore
6. Bennett, J. E. (1974) Chemotherapy of systemic mycoses. *N Engl J Med* **290**, 320-323
7. Vanden Bossche, H. (ed) (1988) *Mode of action of pyridine, pyrimidine and azole antifungals* Vol. 79-119, Ellis Horwood, 79-119, Chichester
8. Maertens, J. A. (2004) History of the development of azole derivatives. *Clin Microbiol Infect* **10**, 1-10
9. Lepesheva, G. I., Villalta, F., and Waterman, M. R. (2011) Targeting *Trypanosoma cruzi* sterol 14α-demethylase (CYP51). *Adv Parasitol* **75**, 65-87
10. Leslie, M. (2011) Drug developers finally take aim at a neglected disease. *Science* **333**, 933-935
11. Docampo, R., Moreno, S. N., Turrens, J. F., Katzin, A. M., Gonzalez-Cappa, S. M., and Stoppani, A. O. (1981) Biochemical and ultrastructural alterations produced by miconazole and econazole in *Trypanosoma cruzi*. *Mol Biochem Parasitol* **3**, 169-180
12. Beach, D. H., Goad, L. J., and Holz, G. G. (1986) Effects of ketoconazole on sterol biosynthesis by *Trypanosoma cruzi* epimastigotes. *Biochem Biophys Res Commun* **136**, 851-856
13. Urbina, J. A., Lazardi, K., Aguirre, T., Piras, M. M., and Piras, R. (1988) Antiproliferative synergism of the allylamine SF 86-327 and ketoconazole on epimastigotes and amastigotes of *Trypanosoma (Schizotrypanum) cruzi*. *Antimicrob Agents Chemother* **32**, 1237-1242
14. Apt, W., Aguilera, X., Arribada, A., Pérez, C., Miranda, C., Sánchez, G., Zulantay, I., Cortés, P., Rodriguez, J., and Juri, D. (1998) Treatment of chronic Chagas' disease with itraconazole and allopurinol. *Am J Trop Med Hyg* **59**, 133-138
15. Araujo, M. S., Martins-Filho, O. A., Pereira, M. E., and Brener, Z. (2000) A combination of benznidazole and ketoconazole enhances efficacy of chemotherapy of experimental Chagas' disease. *J Antimicrob Chemother* **45**, 819-824
16. Molina, J., Martins-Filho, O., Brener, Z., Romanha, A. J., Loebenberg, D., and Urbina, J. A. (2000) Activities of the triazole derivative SCH 56592 (posaconazole) against drug-resistant

strains of the protozoan parasite*Trypanosoma (Schizotrypanum) cruzi* in immunocompetent and immunosuppressed murine hosts. *Antimicrob Agents Chemother* **44**, 150-155
17. Urbina, J. A. (2009) Ergosterol biosynthesis and drug development for Chagas disease. *Mem Inst Oswaldo Cruz* **104 Suppl 1**, 311-318
18. Clayton, J. (2010) Chagas disease: pushing through the pipeline. *Nature* **465**, S12-S15
19. Hucke, O., Gelb, M. H., Verlinde, C. L. M. J., and Buckner, F. S. (2005) The protein farnesyltransferase inhibitor tipifarnib as a new lead for the development of drugs against Chagas disease. *J Med Chem* **48**, 5415-5418
20. Buckner, F., Bahia MT, Suryadevara PK, White KL, Shackleford DM, Chennamaneni NK, Hulverson MA, Laydbak JU, Chatelain E, Scandale I, Verlinde CL, Charman SA, Lepesheva GI, Gelb MH (2012) Pharmacological characterization, structural studies, and in vivo activity of anti-Chagas disease lead compounds derived from tipifarnib. *Antimicrob. Agents Chemother.* **56**, 4914-4921
21. Buckner, F., Yokoyama, K., Lockman, J., Aikenhead, K., Ohkanda, J., Sadilek, M., Sebti, S., Van Voorhis, W., Hamilton, A., and Gelb, M. H. (2003) A class of sterol 14-demethylase inhibitors as anti-*Trypanosoma cruzi* agents. *Proc Natl Acad Sci USA* **100**, 15149-15153
22. Villalta, F., Dobish, M. C., Nde, P. N., Kleshchenko, Y. Y., Hargrove, T. Y., Johnson, C. A., Waterman, M. R., Johnston, J. N., and Lepesheva, G. I. (2013) VNI cures acute and chronic experimental Chagas disease. *J Infect Dis* **208**, 504-511
23. Roberts, C. W., McLeod, R., Rice, D. W., Ginger, M., Chance, M. L., and Goad, L. J. (2003) Fatty acid and sterol metabolism: potential antimicrobial targets in apicomplexan and trypanosomatid parasitic protozoa. *Mol Biochem Parasitol* **126**, 129-142
24. Lazardi, K., Urbina, J. A., and de Souza, W. (1990) Ultrastructural alterations induced by two ergosterol biosynthesis inhibitors, ketoconazole and terbinafine, on epimastigotes and amastigotes of *Trypanosoma (Schizotrypanum) cruzi*. *Antimicrob Agents Chemother* **34**, 2097-2105
25. Lepesheva, G. I., Hargrove, T. Y., Anderson, S., Kleshchenko, Y., Furtak, V., Wawrzak, Z., Villalta, F., and Waterman, M. R. (2010) Structural insights into inhibition of sterol 14 alpha-demethylase in the human pathogen *Trypanosoma cruzi*. *J Biol Chem* **285**, 25582-25590
26. Lepesheva, G. I., Ott, R. D., Hargrove, T. Y., Kleshchenko, Y. Y., Schuster, I., Nes, W. D., Hill, G. C., Villalta, F., and Waterman, M. R. (2007) Sterol 14 alpha-demethylase as a potential target for antitrypanosomal therapy: Enzyme inhibition and parasite cell growth. *Chem Biol* **14**, 1283-1293
27. Lepesheva, G., Hargrove, T., Kleshchenko, Y., Nes, W., Villalta, F., and Waterman, M. (2008) CYP51: A major drug target in the cytochrome P450 superfamily. *Lipids* **43**, 1117-1125
28. Soeiro, M. d. N. C., de Souza, E. M., da Silva, C. F., Batista, D. d. G. J., Batista, M. M., Pavão, B. P., Araújo, J. S., Aiub, C. A. F., da Silva, P. B., Lionel, J., Britto, C., Kim, K., Sulikowski, G., Hargrove, T. Y., Waterman, M. R., and Lepesheva, G. I. (2013) *In vitro* and *in vivo* studies of the antiparasitic activity of sterol 14α-demethylase (CYP51) inhibitor VNI against drug-resistant strains of *Trypanosoma cruzi*. *Antimicrob Agents Chemother* **57**, 4151-4163
29. Lepesheva, G. I., Zaitseva, N. G., Nes, W. D., Zhou, W., Arase, M., Liu, J., Hill, G. C., and Waterman, M. R. (2006) CYP51 from *Trypanosoma cruzi*: a phyla-specific residue in the B' helix defines substrate preferences of sterol 14alpha-demethylase. *J Biol Chem* **281**, 3577-3585
30. Lepesheva, G. I., Nes, W. D., Zhou, W., Hill, G. C., and Waterman, M. R. (2004) CYP51 from *Trypanosoma brucei* is obtusifoliol-specific. *Biochemistry* **43**, 10789-10799
31. Hargrove, T. Y., Wawrzak, Z., Liu, J., Nes, W. D., Waterman, M. R., and Lepesheva, G. I. (2011) Substrate preferences and catalytic parameters determined by structural characteristics of sterol 14α-demethylase (CYP51) from *Leishmania infantum*. *J Biol Chem* **286**, 26838-26848
32. Hargrove, T. Y., Wawrzak, Z., Liu, J., Waterman, M. R., Nes, W. D., and Lepesheva, G. I. (2012) Structural complex of sterol 14α-demethylase (CYP51) with 14α-methylenecyclopropyl-Δ7-24, 25-dihydrolanosterol. *J. Lipid Res.* **53**, 311-320

33. Konkle, M. E., Hargrove, T. Y., Kleshchenko, Y. Y., von Kries, J. P., Ridenour, W., Uddin, M. J., Caprioli, R. M., Marnett, L. J., Nes, W. D., Villalta, F., Waterman, M. R., and Lepesheva, G. I. (2009) Indomethacin amides as a novel molecular scaffold for targeting *Trypanosoma cruzi* sterol 14 alpha-demethylase. *J Med Chem* **52**, 2846-2853
34. Andriani, G., Amata, E., Beatty, J., Clements, Z., Coffey, B. J., Courtemanche, G., Devine, W., Erath, J., Juda, C. E., Wawrzak, Z., Wood, J. T., Lepesheva, G. I., Rodriguez, A., and Pollastri, M. P. (2013) Antitrypanosomal lead discovery: identification of a ligand-efficient inhibitor of *Trypanosoma cruzi* CYP51 and parasite growth. *J Med Chem* **56**, 2556-2567
35. Lepesheva, G. I., Park, H. W., Hargrove, T. Y., Vanhollebeke, B., Wawrzak, Z., Harp, J. M., Sundaramoorthy, M., Nes, W. D., Pays, E., Chaudhuri, M., Villalta, F., and Waterman, M. R. (2010) Crystal structures of *Trypanosoma brucei* sterol 14 alpha-demethylase and implications for selective treatment of human infections. *J Biol Chem* **285**, 1773-1780
36. Lepesheva, G. I., and Waterman, M. R. (2011) Structural basis for conservation in the CYP51 family. *Biochim Biophys Acta* **1814**, 88-93
37. Lepesheva, G. I., and Waterman, M. R. (2011) Sterol 14alpha-demethylase (CYP51) as a therapeutic target for human trypanosomiasis and leishmaniasis. *Curr Top Med Chem.* **11** 2060-2071
38. Keenan, M., Abbott, M. J., Alexander, P. W., Armstrong, T., Best, W. M., Berven, B., Botero, A., Chaplin, J. H., Charman, S. A., Chatelain, E., von Geldern, T. W., Kerfoot, M., Khong, A., Nguyen, T., McManus, J. D., Morizzi, J., Ryan, E., Scandale, I., Thompson, R. A., Wang, S. Z., and White, K. L. (2012) Analogues of fenarimol are potent inhibitors of *Trypanosoma cruzi* and are efficacious in a murine model of Chagas disease. *J Med Chem* **55**, 4189-4204
39. Keenan, M., Alexander, P. W., Diao, H., Best, W. M., Khong, A., Kerfoot, M., Thompson, R. C. A., White, K. L., Shackleford, D. M., Ryan, E., Gregg, A. D., Charman, S. A., von Geldern, T. W., Scandale, I., and Chatelain, E. (2013) Design, structure–activity relationship and in vivo efficacy of piperazine analogues of fenarimol as inhibitors of *Trypanosoma cruzi*. *Bioorg Med Chem* **21**, 1756-1763
40. Buckner, F. S., Verlinde, C. L., La Flamme, A. C., and Van Voorhis, W. C. (1996) Efficient technique for screening drugs for activity against *Trypanosoma cruzi* using parasites expressing beta-galactosidase. *Antimicrob Agents Chemother* **40**, 2592-2597
41. Lepesheva, G. I., Virus, C., and Waterman, M. R. (2003) Conservation in the CYP51 family. Role of the B' helix/BC loop and helices F and G in enzymatic function. *Biochemistry* **42**, 9091-9101
42. Omura, T., and Sato, R. (1964) The carbon monoxide-binding pigment of liver microsomes. I. Evidence for its hemoprotein nature. *J Biol Chem* **239**, 2370-2378
43. Bui, S. H., McLean, K. J., Cheesman, M. R., Bradley, J. M., Rigby, S. E. J., Levy, C. W., Leys, D., and Munro, A. W. (2012) Unusual spectroscopic and ligand binding properties of the cytochrome P450-flavodoxin fusion enzyme XplA. *J Biol Chem* **287**, 19699-19714
44. Leslie, A. (2006) The integration of macromolecular diffraction data. *Acta Crystallogr D Biol Crystallogr* **62**, 48-57
45. Collaborative Computational Project, N. (1994) The CCP4 suite: programs for protein crystallography. *Acta Crystallogr.D Biol. Crystallogr.* **50**, 760-763
46. Emsley, P., Lohkamp, B., Scott, W. G., and Cowtan, K. (2010) Features and development of Coot. *Acta Crystallogr D Biol Crystallogr* **66**, 486-501
47. Vagin, A. A., Steiner, R. S., Lebedev, A. A., Potterton, L., McNicholas, S., Long, F., and Murshudov, G. N. (2004) REFMAC5 dictionary: organisation of prior chemical knowledge and guidelines for its use. *Acta Crystallogr D Biol Crystallogr* **60**, 2284-2295
48. Guengerich, F. P. (2006) Cytochrome P450s and other enzymes in drug metabolism and toxicity. *AAPS J* **8**, E101-E111

49. Lepesheva, G. I., Podust, L. M., Bellamine, A., and Waterman, M. R. (2001) Folding requirements are different between sterol 14α-demethylase (CYP51) from *Mycobacterium tuberculosis* and human or fungal orthologs. *J Biol Chem* **276**, 28413-28420
50. Hargrove, T. Y., Kim, K., de Nazaré Correia Soeiro, M., da Silva, C. F., da Gama Jaen Batista, D., Batista, M. M., Yazlovitskaya, E. M., Waterman, M. R., Sulikowski, G. A., and Lepesheva, G. I. (2012) CYP51 structures and structure-based development of novel, pathogen-specific inhibitory scaffolds. *Int J Parasitol Drugs Drug Resist* **2**, 178-186
51. Correia, M. A., and Ortiz de Montellano, P. R. (2005) Inhibition of cytochrome P450 enzymes. in *Cytochrome P450: Structure, Mechanism, and Biochemistry* (Ortiz de Montellano, P. R. ed.), Plenum Publishing Corp, New York. pp 246-322
52. Zhang, W., Ramamoorthy, Y., Kilicarslan, T., Nolte, H., Tyndale, R. F., and Sellers, E. M. (2002) Inhibition of cytochromes P450 by antifungal imidazole derivatives. *Drug Metab Dispos* **30**, 314-318
53. Obach, R. S., Walsky, R. L., Venkatakrishnan, K., Gaman, E. A., Houston, J. B., and Tremaine, L. M. (2006) The utility of in vitro cytochrome P450 inhibition data in the prediction of drug-drug interactions. *J Pharmacol Exp Ther* **316**, 336-348
54. Schuster, I., and Bernhardt, R. (2007) Inhibition of cytochromes P450: existing and new promising therapeutic targets. *Drug Metab Rev* **39**, 481-499
55. Saari, T. I., and Olkkola, K. T. (2010) Azole antimycotics and drug interactions in the perioperative period. *Curr Opin Anesthesiol* **23**, 441-448
56. Gubbins, P. O. (2011) Triazole antifungal agents drug–drug interactions involving hepatic cytochrome P450. *Expert Opin Drug Metab Toxicol* **7**, 1411-1429
57. Mast, N., Zheng, W., Stout, C. D., and Pikuleva, I. A. (2013) Antifungal azoles: structural insights into undesired tight binding to cholesterol-metabolizing CYP46A1. *Mol Pharmacol* **84**, 86-94
58. Kanafani, Z. A., and Perfect, J. R. (2008) Resistance to antifungal agents: Mechanisms and llinical impact. *Clin Infect Dis* **46**, 120-128
59. Espinel-Ingroff, A. (2008) Mechanisms of resistance to antifungal agents: yeasts and filamentous fungi. *Rev Iberoam Micol* **25**, 101-106
60. Dobish, M. C., Villalta, F., Waterman, M. R., Lepesheva, G. I., and Johnston, J. N. (2012) Organocatalytic, enantioselective synthesis of VNI: A robust therapeutic development platform for Chagas, a neglected tropical disease. *Org Lett* **14**, 6322-6325
61. Strushkevich, N., Usanov, S. A., and Park, H.-W. (2010) Structural basis of human CYP51 inhibition by antifungal azoles. *J Mol Biol* **397**, 1067-1078

FOOTNOTES

*The work on CYP51 was supported by NIH GM 067871 (GIL). For synthesis of EPL-BS1246 (UDO) and EPL-BS0967 (UDD), and their testing in microsomal, cellular experiments and *in vivo* DND*i* received financial support from the following donors: Department for International Development (DFID) / UNITED KINGDOM, Reconstruction Credit Institution-Federal Ministry of Education and Research (KfW-BMBF) / GERMANY, Ministry of Foreign and European Affairs (MAEE) / FRANCE, Spanish Agency for International Development Cooperation (AECID) / SPAIN, Directorate-General for International Cooperation (DGIS)/ NETHERLANDS, Medecins Sans Frontieres (Doctors without Borders) / INTERNATIONAL and a Swiss foundation. The donors had no role in study design, data collection and analysis, decision to publish, or preparation of the manuscript. The contribution of Andrea Khong, and Scott Cornwall from Murdoch University, Murdoch, WA, 6150, Australia, for the testing of the compounds *in vitro* and *in vivo* is greatly acknowledged.

╪The abbreviations used are: CYP, cytochrome P450; CYP51, sterol 14α-demethylase; CPR, cytochrome P450 reductase; *T.*, *Trypanosoma*; *L.*, *Leishmania*; UDO (EPL-BS1246), 2(S)-(4-chloro-phenyl)-1-(4-(4-(trifluoromethyl) phenyl)piperazin-1-yl)-2-(pyridin-3-yl)ethanone; UDD (EPL-BS0967), N-[4-(trifluoromethyl)phenyl]-N-[1-[5-(trifluoromethyl)-2-pyridyl]-4-piperidyl]pyridin-3-amine.

FIGURE LEGENDS

FIGURE 1. Structural formulas and antiparasitic effects of pyridine derivatives EPL-BS1246 (UDO) and EPL-BS0967 (UDD) in comparison with the antifungal drug posaconazole and an experimental *T. cruzi* CYP51 inhibitor VNI. EC_{50} – (effective concentration)$_{50}$, drug concentration required to reduce cellular growth by 50%. ED_{50} (effective dose)$_{50}$, drug regimen required to reach parasitological cure in 50% of animals; IC_{50} (inhibitory concentration)$_{50}$, drug concentration required to inhibit the activity of the enzyme by 50%. qd, once daily administration, bid , twice daily administration. *Data from (22); ** data from (38).

FIGURE 2. 2Fo-Fc electron density map of *T. cruzi* CYP51 in complex with UDO and UDD weighted at 1.5 σ. The distance between Fe^{3+} and the pyridine ring nitrogen (Å) is marked with dashed purple line.

FIGURE 3. Analysis of CYP51 interaction with different iron-coordinating ligands: absolute (upper) and difference (lower) spectra and binding curves (right side insets). Spectral responses of *T. cruzi* CYP51 to pyridine derivatives UDO (**A**) and UDD (**B**), triazole posaconazole (**C**) and imidazole VNI (**D**); *L. infantum* CYP51 to UDO (**E**) and UDD (**F**); and human CYP51 to UDO (**G**) and UDD (**H**). The titration experiments were performed in 5 cm optical path cuvettes at P450 concentration 0.4 μM; titration range 0.1 – 2 μM; titration steps 0.1 μM. The binding curves show absorbance changes per 1 cm optical path per 1 nmol P450.

FIGURE 4. **Inhibitory effects of UDO and UDD on CYP51 activity.** Eburicol, obtusifoliol and lanosterol, final concentration 50 μM) were used as substrates for *T. cruzi*, *L. infantum* and human CYP51s, respectively; molar ratio enzyme/substrate=1/50; 1 hour reaction (no substrate conversion was observed after a 5-min reaction in the presence of each of the compounds at 1/1 molar ratio inhibitor/enzyme). **A**. HPLC profiles of substrate (S) conversion by *T. cruzi* and *L. infantum* CYP51 orthologs in the presence of a 2-fold molar excess of the inhibitors over the enzyme. Posaconazole was used as a control. I1, 14α-carboxyalcohol intermediate, I2, 14α-carboxyaldehyde intermediate; P, 14α-demethylated CYP51 reaction product. **B**. *T. cruzi*; **C.** *L. infantum;* **D**. human CYP51 activity at increasing molar excesses of UDO an UDD.

FIGURE 5. Structural characterization of *T. cruzi* CYP51 complexes with UDO (salmon) and UDD (grey). A. Superimposition of UDO and UDD with posaconazole (yellow) in 3k1o. B. Superimposition of UDO and UDD with VNI (yellow) in 3gw9. C. Overall view of the protein (rainbow color, from blue N terminus to red C terminus) with the bound inhibitors. P450 orientation is the same as in A and B; semitransparent surfaces of UDO and UDD are shown. The surfaces of the inhibitors are shown as semitransparent mesh. D. Distal view of superimposed 3gj2 (salmon), 3gj3 (grey) and 3k1o (gold), ribbon diagram. In 3k1o, the structural elements forming the entrance into the substrate access channel are colored in green.

FIGURE 6. Views of the *T. cruzi* CYP51 active site illustrating interactions with UDO (salmon colored carbon atoms) and UDD (grey colored carbon atoms). A. Binding of UDO. The inhibitor molecule is shown as a sphere model, the carbon atoms of the side chains of the inhibitor contacting amino acid residues are depicted as light blue stick models; the corresponding secondary structural elements are shown as semitransparent grey ribbons and numbered; the C-atoms of the heme are yellow. UDO-specific *T. cruzi* CYP51 residues are underlined. **B**. Binding of UDD (sphere model, grey colored carbon atoms). The carbon atoms of the side chains of the inhibitor contacting residues and the semitransparent ribbon of the corresponding secondary structural residues are colored in pink and numbered. UDD-specific *T. cruzi* CYP51 residues are underlined. **C**. Comparative location of the inhibitor-contacting residues in the superimposed *T. cruzi* CYP51 co-structures with UDO and UDD. P450 orientation is the same as in **A**, **B**. Stereo view. The side chains of the inhibitor contacting residues

remain in very similar positions, with only long arms of M106 and M460 being shifted to the right in the UDO structure to better accommodate piperazinyl ring of the inhibitor. **D**. While both conserved in the CYP51 family heme supporting hydrogen bonds, between the hydroxyl Y103 and the porphyrin ring A propionate as well as between Y116 and the porphyrin ring D propionate, are preserved in the *T. cruzi* CYP51 complex with UDO, binding of UDD requires wedging of its aromatic ring between Y116 and the heme plane, which results in the Y116 OH - porphyrin ring D hydrogen bond disruption.

FIGURE 7. Structural explanation for UDO/UDD pathogen-selectivity. **A**. F104 in the *L. infantum* CYP51 structure (3l4d) relative to I105 in the superimposed *T. cruzi* CYP51 (3zg3). At 72% average amino acid sequence identity, *L. infantum* and *T. cruzi* have only one amino acid difference in the residues whose side chains line the surface of the substrate binding cavity. **B**. Twelve amino acid differences inside the substrate binding cavity in *T. cruzi* (3zg2) and human (3ld3 (61)) CYP51s. UDO, UDD, the heme and 6 iron coordination bonds including the thiolate of C422 (the fifth (proximal) iron ligand) are shown. Color code for *T. cruzi* CYP51 structures is the same as in Fig.6. *L. infantum* and human CYP51s are colored in cyan and tan, respectively.

Table 1. Inhibitory effects of UDO and UDD on five major drug metabolizing CYPs determined in human liver microsomes

CYP	substrate	Substrate conc. (μM)[a]	Metabolic Pathway	Microsomal protein conc. (mg/mL)	Assay incubation duration (min)[b]	UDD IC_{50} (μM)	UDO IC_{50} (μM)
1A2	phenacetin	40	phenacetin-O-deethylation	0.4	30	>20	>20
2C9	tolbutamide	140	tolbutamide methylhydroxylation	0.4	20	8.1	9
2C19	S-mephenytoin	30	S-mephenytoin 4'-hydroxylation	1.0	40	9.8	12
2D6	dextrometho rphan	3	dextromethorphan O-deethylation	0.4	10	20	4
3A4	testosterone	50	testosterone-6-β-hydroxylation	0.4	5	>20	20

[a] Substrate concentrations were ≤ K_m values.

[b] For each CYP, enzyme kinetic studies confirmed linear metabolite formation over this time period using the stated conditions.

Table 2. Data collection and refinement statistics

T. cruzi CYP51-inhibitor complex	EPL-BS1246 [UDO] [3zg2]	EPL-BS0967 [UDD] [3zg3]
Data collection		
Wavelength, Å	0.9786	0.9786
Space group	P3(1)21	P3(1)21
Cell dimensions		
a, b, c, Å	63.699;63.699;223.263	62.849;62,849;222.395
α, β, γ, °	90.00, 90.00, 120.00	90.00, 90.00, 120.00
Molecules per asymmetric unit	1	1
Solvent content, %	50.2	48.6
Resolution (last shell), Å	30-2.8 (2.9-2.8)	74-2.9 (3.0-2.9)
R_{merge} (last shell)	0.043 (0.523)	0.085 (587)
I/σ (last shell)	69.4 (3.9)	21.3(2.4)
Completeness (last shell), %	99.3 (100)	99 (100)
Redundancy (last shell)	21.2 (6.9)	6.9 (7.1)
Refinement		
Resolution, Å	27.7-2.8	30.0-2.9
R-factor	0.268	0.248
R-free	0.282	0.289
Reflections used	12182	11342
Test set size, %	5.3	5.3
Rms deviations from ideal geometry		
Bond lengths, Å	0.003	0.003
Bond angles, °	1.23	0.716
Ramachandran plot		
Residues in favorable regions (%)	95.7	96.8
Residues in allowed regions (%)	100	100
Outliers (%)	0	0
Model		
Number of atoms (average B-factor, Å)	3677 (58.1)	3639 (114.5)
Residues		
protein	448 (58.6)	445 (115.3)
heme	1 (26.6)	1 (65.0)
Ligand	1 (38.9)	1 (90.2)
Water	13 (57.1)	6 (135.0)

Table 3. Apparent binding parameters and inhibition of *T. cruzi*, *L. infantum* and human CYP51 activity by UDO and UDD.

CYP51- inhibitor	Binding parameters			Inhibitor/enzyme molar ratio required for a two-fold decrease in CYP51 activity (1 h reaction)
	K_d (μM)	ΔA_{max}/cm/nmol P450 (o.u.)	$\Delta A_{max}/K_d$	
T. cruzi – UDO	0.019±0.002	0.039±0.0002	2.0	<1
T. cruzi – UDD	0.032±0.002	0.040±0.0002	2.0	<1
T. cruzi – posaconazole	0.018±0.001	0.043±0.0001	2.4	<1
T. cruzi – VNI	0.015±0.002	0.047±0.0002	3.1	<1
L. infantum – UDO	0.156±0.006	0.036±0.0003	0.2	1.5
L. infantum – UDD	0.419±0.019	0.043±0.0006	0.1	2.8
L. infantum – posaconazole	0.018±0.001	0.037±0.0001	2.1	<1
Human – UDO	0.069±0.003	0.034±0.0001	0.5	180
Human – UDD	0.026±0.002	0.046±0.0001	1.8	35

Table 4. Correlation between the spectral properties and the distances between the heme Fe and coordinating N atoms in the CYP51 complexes with imidazole, triazole and pyridine derivatives

Sixth (distal) ligand of the heme iron		Absorbance (nm)*				Coordination bond (Å)
Fe-coordinating atom	Compound [PDB ID]	Soret band maximum	Difference spectrum			
			trough	isosbestic point	peak	
Imidazole N3	VNI [3gw9]	424	407	419	428	2.00
Triazole N4	Posaconazole [3k1o]	423	392	415	426	2.07
Pyridine N	UDO [3zg2]	421	389	411	423	2.31
	UDD [3zg3]	421	389	411	422	2.34
Water O	HOH [3g1q]	417	-	-	-	2.93

*the spectra are shown in Fig. 3.

Figure 1

EPL-BS1246 (UDO)

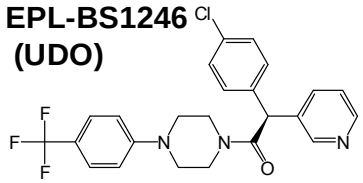

T. cruzi (Tulahuen) amastigotes: EC_{50}=7.5 nM
acute Chagas mouse model: ED_{50}=20mg/kg/qd for 20 days

L. donovani: not tested

CYP3A4: IC_{50} >16 µM

EPL-BS0967 (UDD)

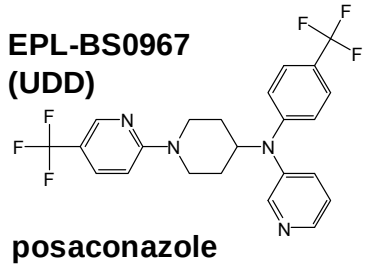

T. cruzi (Tulahuen) amastigotes: EC_{50}=15 nM
acute Chagas mouse model: ED_{50}=20mg/kg/qd for 20 days

L. donovani: EC_{50} >10 µM (EC_{38}=10 µM)

CYP3A4: IC_{50}> 16 µM

posaconazole

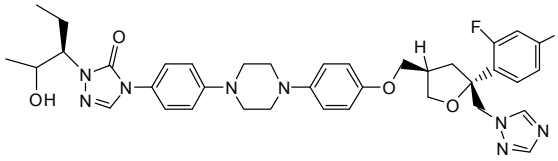

T. cruzi (Tulahuen) amastigotes: EC_{50}=5 nM*
acute Chagas mouse model: ED_{60}=20mg/kg/qd for 20 days**

CYP3A4: IC_{50}=0.120 µM

VNI

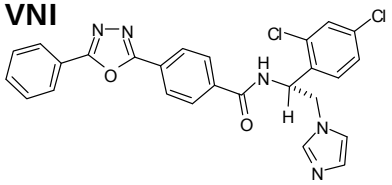

T. cruzi (Tulahuen) amastigotes: EC_{50}=1.3 nM*
acute Chagas mouse model: ED_{100}=25mg/kg/bid for 30 days*
CYP3A4: IC_{50}=0.405 µM

Figure 2

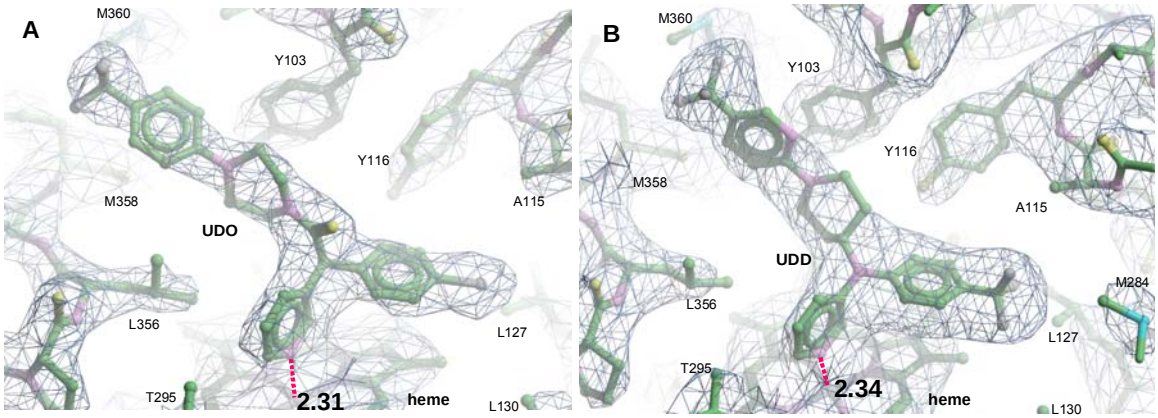
A
M360
Y103
Y116
M358
A115
UDO
L356
L127
T295
2.31
heme
L130
B
M360
Y103
Y116
M358
A115
UDD
M284
L356
L127
T295
2.34
heme
L130

Figure 3

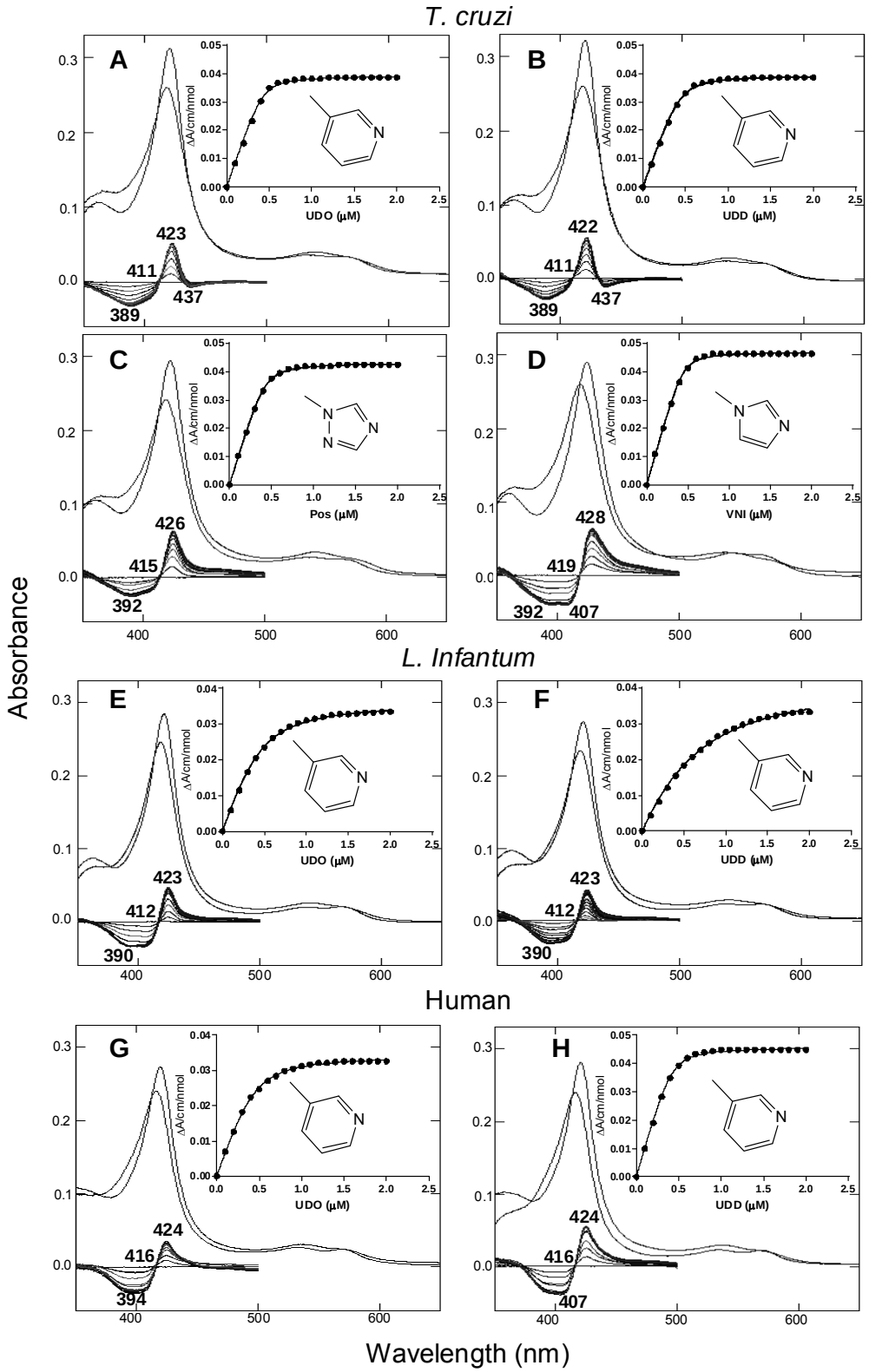
T. cruzi
A
B
C
D
L. Infantum
E
F
Human
G
H
UDO (μM)
UDD (μM)
Pos (μM)
VNI (μM)
ΔA/cm/nmol
Absorbance
Wavelength (nm)
423
411
437
389
422
411
437
389
426
415
392
428
419
392
407
423
412
390
423
412
390
424
416
394
424
416
407

Figure 4

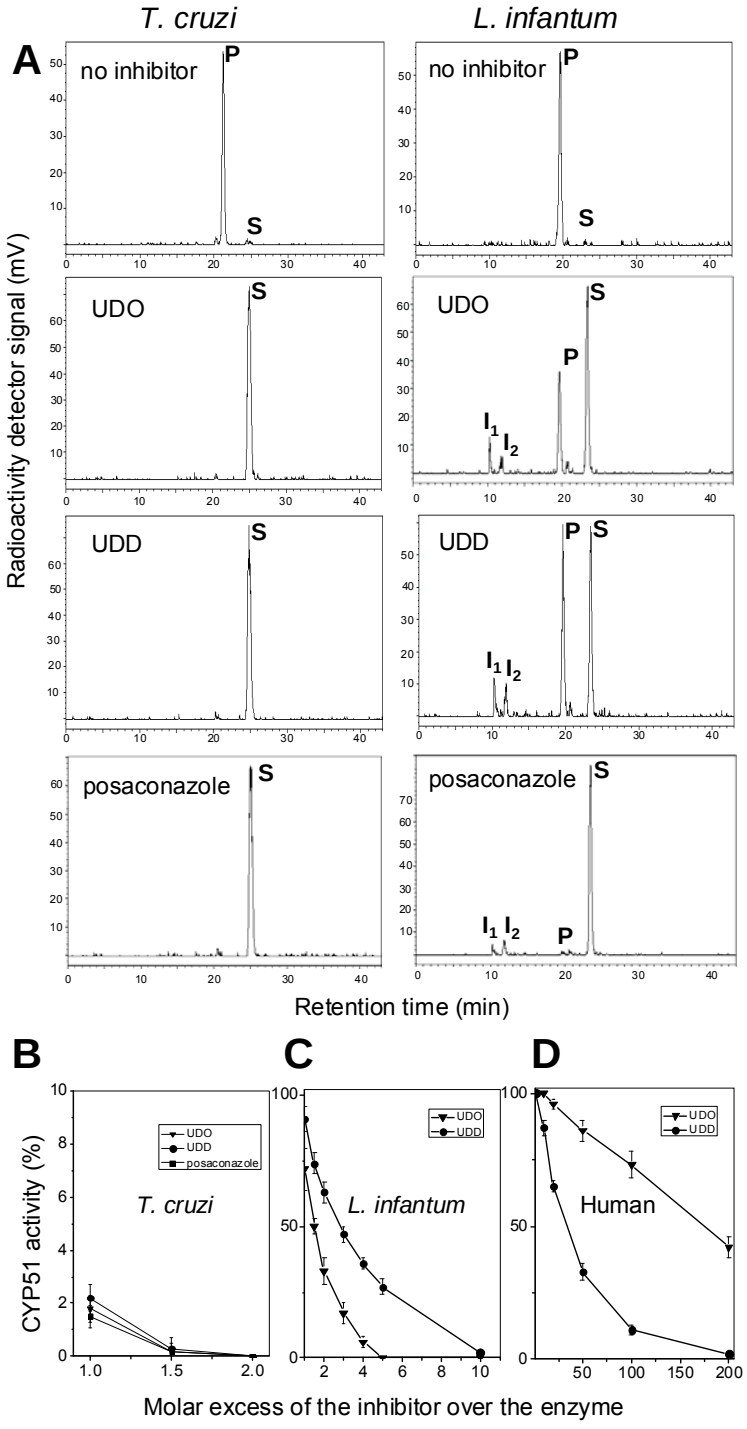
T. cruzi
L. infantum
A
no inhibitor
UDO
UDD
posaconazole
P
S
I1
I2
Radioactivity detector signal (mV)
Retention time (min)
B
C
D
CYP51 activity (%)
UDO
UDD
posaconazole
T. cruzi
L. infantum
Human
Molar excess of the inhibitor over the enzyme

Figure 5

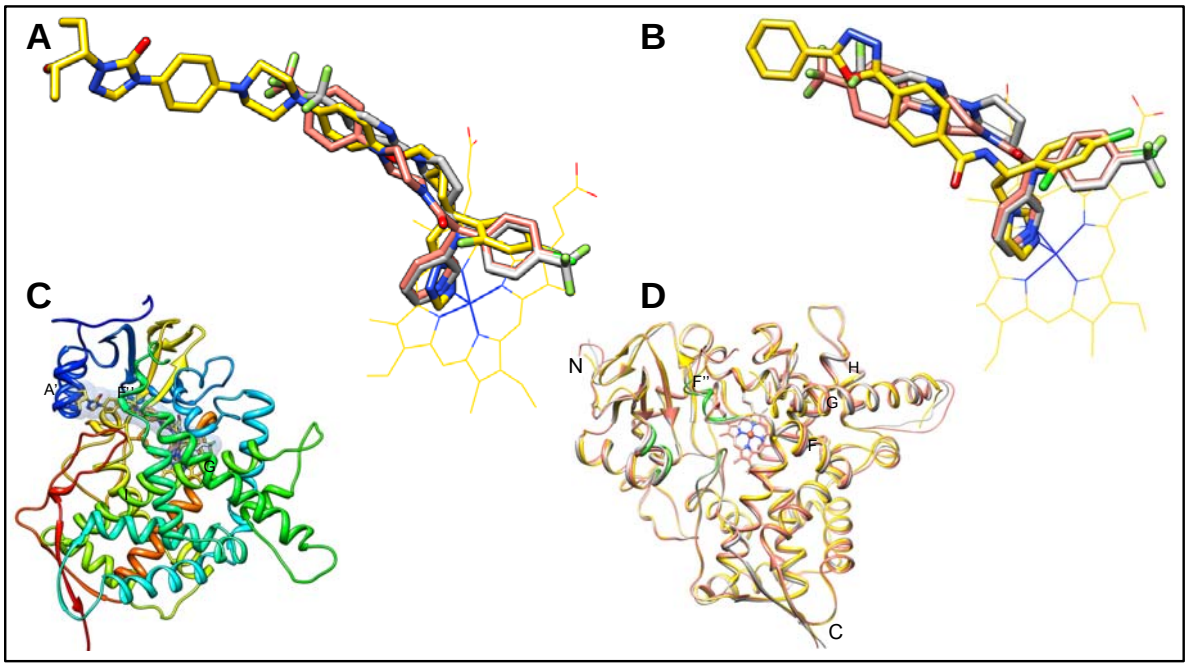

Figure 6

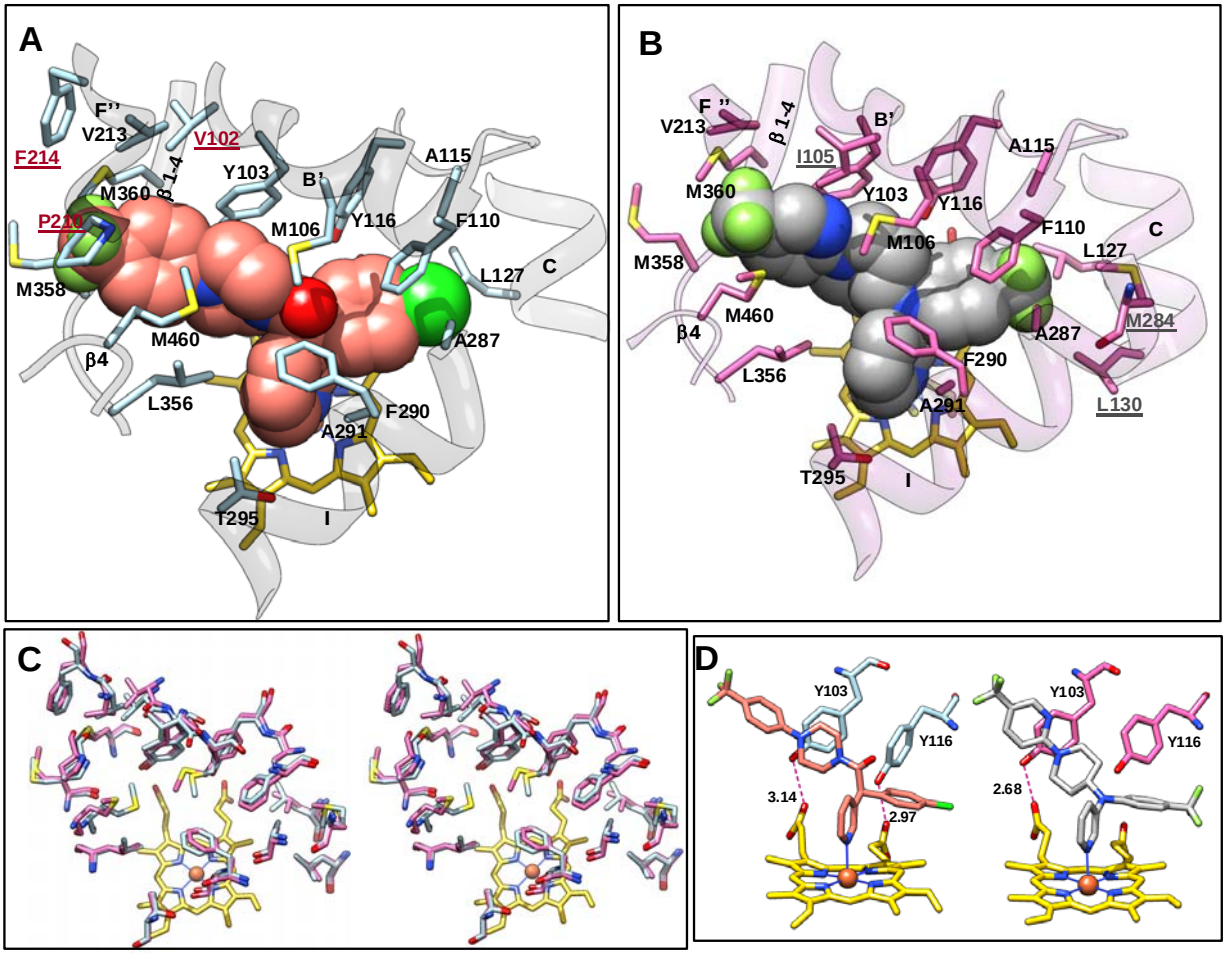
A
F''
V213
V102
F214
β1-4
Y103
B'
A115
M360
P230
M106
Y116
F110
C
L127
M358
M460
A287
β4
L356
F290
A291
T295
I
B
F''
V213
β1-4
B'
I105
A115
M360
Y103
Y116
M106
F110
C
L127
M358
M460
M284
β4
A287
F290
L356
A291
L130
T295
I
C
D
Y103
Y116
3.14
2.97
Y103
Y116
2.68

Figure 7

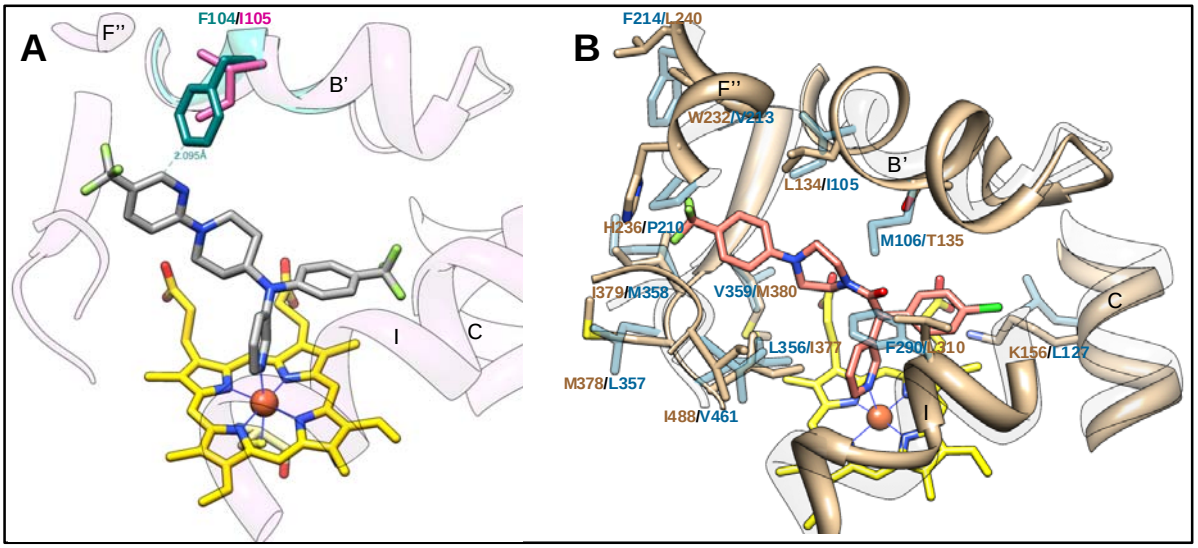
A
F''
F104/I105
B'
2.095Å
I
C
B
F214/L240
F''
W232/Y223
B'
L134/I105
H236/P210
M106/T135
I379/M358
V359/M380
C
L356/I377
F290/L310
K156/L127
M378/L357
I488/V461
I